Improved Accuracy and Robustness of a Corneal Endothelial Cell Segmentation Method Based on Merging Superpixels

Vigueras-Guillén, Juan P.; Engel, Angela; Lemij, Hans G.; van Rooij, Jeroen; Vermeer, Koenraad A.; van Vliet, Lucas J.

DOI
10.1007/978-3-319-93000-8_72

Publication date
2018

Document Version
Final published version

Published in
Image Analysis and Recognition - 15th International Conference, ICIAR 2018, Proceedings

Citation (APA)
Vigueras-Guillén, J. P., Engel, A., Lemij, H. G., van Rooij, J., Vermeer, K. A., & van Vliet, L. J. (2018). Improved Accuracy and Robustness of a Corneal Endothelial Cell Segmentation Method Based on Merging Superpixels. In *Image Analysis and Recognition - 15th International Conference, ICIAR 2018, Proceedings* (Vol. 10882 LNCS, pp. 631-638). (Lecture Notes in Computer Science (including subseries Lecture Notes in Artificial Intelligence and Lecture Notes in Bioinformatics); Vol. 10882 LNCS). Springer. https://doi.org/10.1007/978-3-319-93000-8_72

Improved Accuracy and Robustness of a Corneal Endothelial Cell Segmentation Method Based on Merging Superpixels

Juan P. Vigueras-Guillén[1,3(✉)], Angela Engel[1], Hans G. Lemij[2], Jeroen van Rooij[2], Koenraad A. Vermeer[1], and Lucas J. van Vliet[3]

[1] Rotterdam Ophthalmic Institute, Rotterdam, The Netherlands
[2] The Rotterdam Eye Hospital, Rotterdam, The Netherlands
[3] Department of Imaging Physics, Delft University of Technology, Delft, The Netherlands
J.P.ViguerasGuillen@tudelft.nl

Abstract. Clinical parameters related to the corneal endothelium can only be estimated by segmenting endothelial cell images. Specular microscopy is the current standard technique to image the endothelium, but its low SNR make the segmentation a complicated task. Recently, we proposed a method to segment such images by starting with an oversegmented image and merging the superpixels that constitute a cell. Here, we show how our merging method provides better results than optimizing the segmentation itself. Furthermore, our method can provide accurate results despite the degree of the initial oversegmentation, resulting into a precision and recall of 0.91 for the optimal oversegmentation.

Keywords: Specular microscopy · Oversegmentation · Watershed

1 Introduction

The endothelium of the cornea, a monolayer of hexagonal shaped cells on the posterior corneal surface, plays a key role in keeping an optimal state of corneal hydration [2]. Human endothelial cell density decreases naturally with increasing age, and regeneration of endothelial cells has not been observed under normal circumstances. Instead, endothelial cells grow and migrate to occupy the space that is freed by the dying cells. Intraocular surgery, trauma, and certain diseases may accelerate cell loss. If cell density drops below 700 cells/mm^2, the resulting corneal edema may disrupt vision [3]. Accurate quantification of the endothelial cell morphology is crucial for the assessment of the health status of the cornea.

Non-contact specular microscopy and contact confocal microscopy are commonly used in clinical practice to image the endothelium *in vivo*. Characterized by its non-invasive nature and fast acquisition time, non-contact specular

This work was supported by ZonMw under Grants 842005004 and 842005007.

A. Campilho et al. (Eds.): ICIAR 2018, LNCS 10882, pp. 631–638, 2018.
https://doi.org/10.1007/978-3-319-93000-8_72

microscopy provides reliable and reproducible measurements [8]. In comparison, contact confocal microscopy requires corneal contact and has longer acquisition time, but it provides higher quality endothelial images in diseased and edematous corneas [5]. Furthermore, ocular microsaccades, respiration, and pulse are important, limiting factors in the acquisition of good quality images *in vivo*.

Endothelial cell density (ECD), cell size variation (CV), and hexagonality (HEX) are the three main parameters to assess the endothelium. Microscope manufacturers provide built-in software to automatically segment endothelium images and estimate these parameters. However, many studies have indicated that current microscope software may provide unreliable estimations, specifically in the cases with low or high cell density or a high degree of CV [6–8].

In recent years, several cell segmentation techniques for *in vivo* corneal endothelium images were proposed. More studies were focused on segmenting confocal images [10,11] rather than specular [9], probably because of its better image quality and signal-to-noise ratio (SNR). Hence, there is a need to develop algorithms that can accurately segment specular microscopy endothelial images.

1.1 Our Aim

We have recently developed an automatic algorithm to segment *in vivo* specular microscopy images [12]. Briefly summarized, our method aims to generate an accurate segmentation by starting with an oversegmented endothelial cell image and merging those superpixels that together comprise a whole cell (Fig. 1). We showed how a machine learning approach (based on Support Vector Machines) can use features related to shape, intensity, size, etc., to identify the superpixels that constitute a complete cell. During the merging process, all combinations of two and three neighboring superpixels are evaluated simultaneously, using a dedicated classifier for the merger of two or three superpixels. The binary classification is then transformed into a probabilistic output, which allows to sort the combinations. In a iterative process, the combination with the highest probability is merged until no more acceptable combinations ($p > 0.5$) remain.

Although any method that can generate oversegmented endothelial cell images could be used as a starting point, we chose to adapt Selig *et al.*'s approach [10] because of its simplicity to generate and adjust oversegmentation. Selig *et al.* designed a seeded watershed algorithm in a stochastic manner to segment *in vivo* confocal microscopy images, which requires fine-tuning of several parameters in order to achieve a satisfactory result. In our approach [12], parameter tuning was not necessary as we aimed for oversegmentation.

In this paper, we show how our method can improve the accuracy of Selig *et al.*'s [10] optimal segmentation when applied to *in vivo* specular microscopy images. By using precision and recall to evaluate the segmentation, we obtained the best parameter values for Selig *et al.*'s method and computed the corresponding segmentation (named "*watershed optimized result*"). After applying our merging method [12] to the watershed optimized result, we evaluated the segmentation results. Furthermore, we generated several oversegmented images with different degrees of oversegmentation, applied our merging method to all of

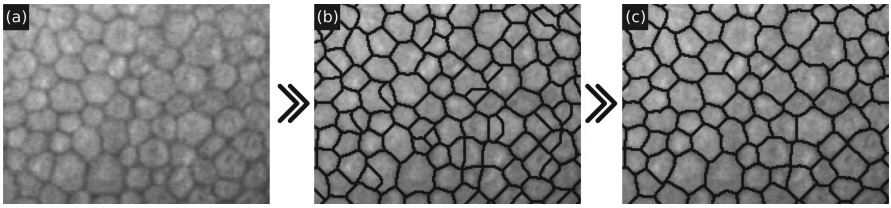

Fig. 1. (a) Input image. (b) Initial oversegmentation. (c) Output of merging process.

them, and evaluated the resulting segmentation, thereby showing the robustness of our method against various degrees of oversegmentation.

2 Method

2.1 Materials

The dataset contains 30 corneal endothelium images from the central cornea of 30 glaucomatous eyes, acquired in The Rotterdam Eye Hospital with a non-contact specular microscope (SP-1P, Topcon, Japan) for an ongoing study regarding the implantation of a Baerveldt glaucoma drainage device. Each image covers an area of $0.25\,\text{mm} \times 0.55\,\text{mm}$ and they were saved as 8-bits grayscale images of 241×529 pixels. The dataset shows a large variability in cell morphology, with a range of 1400–2700 cells/mm^2 in ECD, 19%–35% in CV, and 44%–73% in HEX. The acquisition occurred with informed consent and followed the tenets of the Declaration of Helsinki. One expert created the gold standard by performing manual segmentation of the edges using an image manipulation program, GIMP.

2.2 Description of Selig *et al.*'s Method

Selig *et al.*'s method [10] employs a seeded stochastic watershed algorithm to segment endothelial cell images. The seeds are arranged in a hexagonal grid to mimic the endothelial cells pattern. The grid size is derived by estimating the most common cell size, which can be computed from the Fourier spectrum of the image (see Sect. 2.3). The seeded watershed algorithm is repeatedly applied, $m = 100$ times (value derived in [1]), to a randomly rotated and translated grid. Uniformly distributed noise in the range of $[0, u]$ is added to the image at each iteration, which avoids the occurrence of spurious segmentation lines [1]. The result of all seeded watershed segmentations are summed together, providing an image named *likelihood map* (or PDF), which indicates how often each pixel was selected as edge. To smooth the result, a Gaussian smoothing filter is applied to the PDF, whose optimal σ_{PDF} is related to the cell size. To adapt σ_{PDF} to the cell size of each image, Selig *et al.* defined a parameter $k_\sigma = \sigma_{PDF} f^*$, where f^* is the characteristic frequency estimated from the Fourier spectrum of the image. An H-minima transform is then applied to the PDF, $h = k_h m / \sigma_{PDF}$, to discard small minima. Finally, the classical watershed is applied to the PDF,

resulting in the final segmentation. Selig *et al.* observed that the smoothing was very sensitive to errors in the estimation of f^*, and so they suggested to re-estimate f^* from the PDF. In summary, three parameters are to be tuned in the algorithm: noise amplitude u, smoothing size k_σ, and local minima depth k_h.

2.3 Frequency Analysis

The 2D Fourier transform (2D FT) of an endothelial image shows a distinctive concentric ring due to the fairly regular size and pattern of the cells [4]. The ring's radius, called *characteristic frequency* (f^*), is related to the most common cell size in the image, $l = 1/f^*$ [10]. To determine the radius, we compute the 1D radial magnitude by angular averaging of the magnitude of the 2D FT,

$$\mathcal{F}_{RM}(f) = \frac{1}{2\pi} \int_0^{2\pi} |\mathcal{F}(f, \theta)| d\theta, \tag{1}$$

where $\mathcal{F}(f, \theta)$ is the Fourier transform of the intensity image in polar coordinates. Thus, the ring radius in the 2D FT appears as a peak in the 1D radial magnitude. Since specular microscopy images have lower SNR, lower contrast, and lower resolution than confocal images, the ring appears almost imperceptible in the radial magnitude (Fig. 2a, arrow). Selig *et al.* [10] proposed a method, named reconstruction by dilation, to enhance the peak (Fig. 2b) and find its value by fitting a parabola. While the enhancement method works well in specular microscopy images, the parabola fitting must be applied with caution because it is prone to generate wrong estimations. Instead, we propose to fit a function that is comprised of a decaying exponential and a Gaussian,

$$g(f; a, b, c, \mu, \sigma) = a \exp(-bf) + \frac{1}{\sqrt{2\pi\sigma^2}} \exp\left(\frac{-(f-\mu)^2}{2\sigma^2}\right) + c, \tag{2}$$

where g is the model, f is the spatial frequency, a and b are the scale parameters of the exponential, μ and σ are the mean and standard deviation of the Gaussian respectively, and c is the offset. A non-linear least-squares solver was used to find the parameters. The characteristic frequency is then estimated as the position of the Gaussian (μ). As suggested by Selig *et al.* [10], the estimation of f^* can be improved if the model is fitted to the Fourier transform of the PDF (Fig. 2c).

2.4 Generating Oversegmentation

Oversegmentation can easily be induced by creating a denser grid of seeds in Selig *et al.*'s method [10]. Given the total image area A_I, the expected number of cells in the image is $n_{seeds} = NA_I f^{*2}$, with $N = 1$ for the watershed optimized segmentation. In our merging method, we used a value $N = 3$, which is equivalent to a three times higher cell density. In this paper, we generate nine oversegmented images by taking the integer values $N = 1, 2, ..., 9$.

Two scenarios to create oversegmentation were considered. If f^* is reestimated in the PDF after oversegmentation was applied, the frequency spectrum will show the components of the smaller superpixels in the PDF (Fig. 2d). Then,

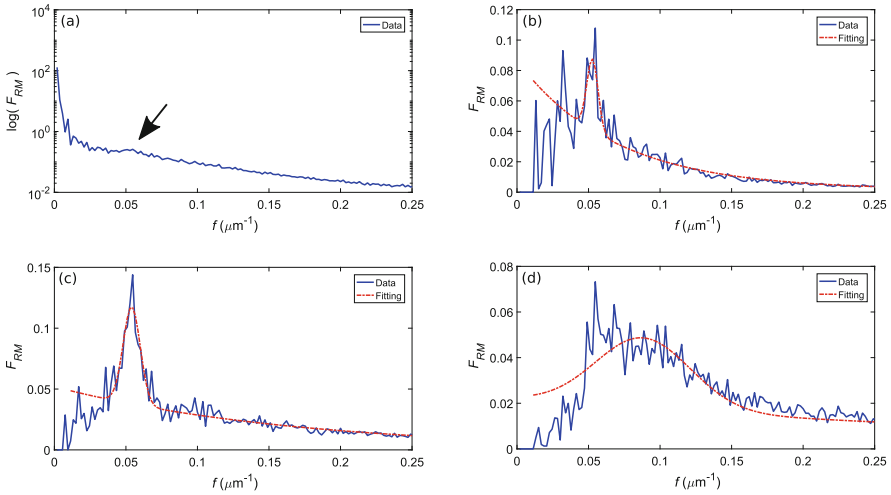

Fig. 2. The radial magnitude of the FT after angular averaging at different stages of preprocessing in order to estimate f^*. (a) No preprocessing; f^* is almost indiscernible (arrow). (b) After reconstruction by dilation in the FT of the image (fitting gives a $f^* = 0.0527$). (c) After reconstruction by dilation in the FT of the PDF (fitting indicates a $f^* = 0.0541$). (d) After reconstruction by dilation in the FT of the PDF where an oversegmentation with $N = 8$ was applied (fitting provides a $f^* = 0.0880$).

the fitting function will provide an f^* balanced between the average cell size and the smaller superpixels in the PDF. This simply creates a higher degree of oversegmentation with more irregular sizes of superpixels. Alternatively, we can avoid re-estimation (or to re-estimate it using $N = 1$). Nonetheless, both cases were evaluated here, named *oversg. 1* for the former (re-estimation of f^* in the PDF) and *oversg. 2* for the latter. The degree of oversegmentation in both cases is indicated in Table 1.

2.5 Evaluating the Segmentation

In order to evaluate the segmentation, we computed two values from the segmented images, the total number of superpixels (n_{total}) and the number of cells correctly segmented (n_{corr}), as well as one value from the gold standard, the number of real cells (n_{real}). We considered a cell is correctly segmented based on the following rule: given the area of a cell in the segmentation A_S, the area of a cell in the gold standard A_G, and the intersection of those two areas $A_I = A_S \cap A_G$, the cell in the segmentation is correctly segmented if $A_I > 0.75 \times max(A_S, A_G)$. That margin was added to allow small deviations in the cell boundary locations and was selected after visual analysis.

The precision $p = n_{corr}/n_{total}$ and the recall $r = n_{corr}/n_{real}$ were computed and combined into the F-measure, $F = 2pr/(p + r)$. Although both, over- and under-segmented cells affect both metrics, precision decreases more acutely with oversegmentation and recall decreases more strongly with undersegmentation.

Table 1. Estimated precision and recall for different degrees of oversegmentation (N). The percentage indicates the number of superpixels in the initial oversegmented images relative to N = 1. Watershed optimized result (WOR) is added for comparison purposes.

N	WOR	1	2	3	4	5	6	7	8	9
Oversg. 1 (%)	-	1	1.12	1.24	1.42	1.70	2.04	2.21	2.45	2.68
Precision	0.83	0.89	0.91	0.91	0.91	0.90	0.89	0.88	0.88	0.86
Recall	0.85	0.86	0.90	0.91	0.91	0.91	0.92	0.92	0.92	0.90
Oversg. 2 (%)	-	1	1.10	1.20	1.28	1.35	1.39	1.42	1.44	1.47
Precision	0.83	0.89	0.91	0.91	0.89	0.89	0.88	0.86	0.85	0.85
Recall	0.85	0.86	0.90	0.90	0.89	0.89	0.88	0.86	0.85	0.85

3 Results and Discussion

3.1 Watershed Optimized Result

Selig *et al.*'s algorithm was applied to all images in the dataset for all values of u between 0 and 50 in steps of 10, values of k_σ between 0.10 and 0.25 in steps of 0.01, and values of k_h between 0.000 and 0.010 in steps of 0.001. The F-measure was computed for each image. In a leave-one-out approach, the parameters for image i were estimated as the ones that yielded the largest average F when computed for all images in the dataset excluding i. For all images, the optimal parameters were the same: $u_i = 20$, $k_{\sigma,i} = 0.20$, and $k_{h,i} = 0$.

When evaluated the segmentation without merging, the mean and standard deviation of the precision and recall with the optimal parameters were $p = 0.83 \pm 0.07$ and $r = 0.85 \pm 0.06$, yielding $F = 0.84 \pm 0.07$. This suggested that over- as well as under-segmentation were present.

3.2 Solving the Oversegmentation

Based on the optimal parameters obtained in Sect. 3.1, nine oversegmented images (per image in the dataset) were generated for each type of oversegmentation (as described in Sect. 2.4) after which the merging method [12] was applied to all of them without retraining. The evaluation of the resulting segmentations shows that the watershed optimized result can be directly improved by just applying our merging method (WOR vs. $N = 1$, in Table 1). In a visual evaluation (Fig. 3b, f), it is clear that the watershed optimized result generates under- (red arrows) and over-segmentation (magenta edges). Whereas the latter is mostly solved by the merging method (large increase in precision from WOR to $N = 1$ in Table 1), the former cannot be easily fixed as the number of possible splits grows exponentially with the number of edge pixels per undersegmented superpixel. It is then crucial for our merging method to start with an oversegmented image where no undersegmentation occurs.

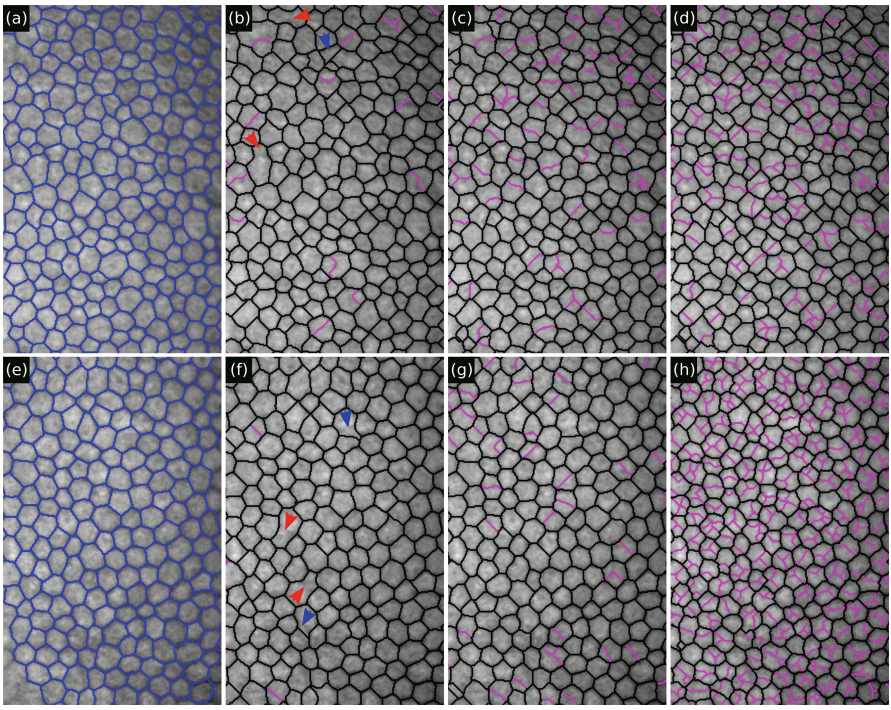

Fig. 3. Two representative examples: *oversg. 2* in (a–d), and *oversg. 1* in (e–h). (a, e) Gold standard segmentation in blue, superimposed over the intensity image. (b, c, d, f, g, h) Resulting segmentation in black, and edges removed during merging process in magenta, for an oversegmentation of $N = 1$ in (b, f), $N = 3$ in (c, g), and $N = 9$ in (d, h). Note that watershed optimized result is (b, f) with all edges (black and magenta). Red arrows indicate undersegmentation. Blue arrows indicate inaccurate segmentation. (Color figure online)

The optimal degree of oversegmentation occurs at $N = 3$ for both types of oversegmentation ($F_{oversg.1} = 0.910$, and $F_{oversg.2} = 0.906$). All true edges seem to be detected at that point, and the degree of oversegmentation is not excessive. For higher values of N, it would be expected that more (presumably unnecessary) initial oversegmentation would only increase the chances of more errors. Interestingly, this hardly happens for the cases in *oversg. 1*. The reason lies in the inaccurate segmentation of some edges due to a limitation of the stochastic watershed: when a strong false edge is detected close to a real edge (blue arrows in Fig. 3f), the latter cannot be detected unless we force a large amount of oversegmentation (Fig. 3h). Whereas such a degree of oversegmentation would suggest a higher error probability, the merging method can satisfactorily overcome this problem. Nonetheless, this evaluation suggests that the best setup is using *oversg. 1* with $N = 3$, as it is more robust.

In summary, we have shown how a segmentation method based on merging superpixels can improve the accuracy of another segmentation method specifically designed to solve confocal images. Furthermore, we have proven how such a merging method is strongly robust against the degree of initial oversegmentation without requiring any retraining.

References

1. Bernander, K.B., Gustavsson, K., Selig, B., Sintorn, I.M., Luengo Hendriks, C.L.: Improving the stochastic watershed. Pattern Recogn. Lett. **34**(9), 993–1000 (2013). https://doi.org/10.1016/j.patrec.2013.02.012
2. Bourne, W.M.: Biology of the corneal endothelium in health and disease. Eye (Lond.) **17**(8), 912–918 (2003). https://doi.org/10.1038/sj.eye.6700559
3. Bourne, W.M., McLaren, J.W.: Clinical responses of the corneal endothelium. Exp. Eye Res. **78**(3), 561–572 (2004). https://doi.org/10.1016/j.exer.2003.08.002
4. Foracchia, M., Ruggeri, A.: Automatic estimation of endothelium cell density in donor corneas by means of fourier analysis. Med. Biol. Eng. Comput. **42**(5), 725–731 (2004). https://doi.org/10.1007/BF02347557
5. Hara, M., Morishige, N., Chikama, T., Nishida, T.: Comparison of confocal biomicroscopy and noncontact specular microscopy for evaluation of the corneal endothelium. Cornea **22**(6), 512–515 (2003). https://doi.org/10.1097/00003226-200308000-00005
6. Hirneiss, C., Schumann, R.G., Gruterich, M., Welge-Luessen, U.C., Kampik, A., Neubauer, A.S.: Endothelial cell density in donor corneas: a comparison of automatic software programs with manual counting. Cornea **26**(1), 80–83 (2007). https://doi.org/10.1097/ICO.0b013e31802be629
7. Huang, J., Maram, J., Tepelus, T.C., Sadda, S.R., Chopra, V., Lee, O.L.: Comparison of noncontact specular and confocal microscopy for evaluation of corneal endothelium. Eye Contact Lens (2017). https://doi.org/10.1097/ICL.0000000000000362
8. Salvetat, M.L., Zeppieri, M., Miani, F., Parisi, L., Felletti, M., Brusini, P.: Comparison between laser scanning in vivo confocal microscopy and noncontact specular microscopy in assessing corneal endothelial cell density and central corneal thicknes. Cornea **30**(7), 754–759 (2011). https://doi.org/10.1097/ICO.0b013e3182000c5d
9. Scarpa, F., Ruggeri, A.: Development of a reliable automated algorithm for the morphometric analysis of human corneal endothelium. Cornea **35**(9), 1222–1228 (2016). https://doi.org/10.1097/ICO.0000000000000908
10. Selig, B., Vermeer, K.A., Rieger, B., Hillenaar, T., Luengo Hendriks, C.L.: Fully automatic evaluation of the corneal endothelium from in vivo confocal microscopy. BMC Med. Imaging **15**, 1–13 (2015). https://doi.org/10.1186/s12880-015-0054-3
11. Sharif, M.S., Qahwaji, R., Shahamatnia, E., Alzubaidi, R., Ipson, S., Brahma, A.: An efficient intelligent analysis system for confocal corneal endothelium images. Comput. Methods Programs. Biomed. **122**(3), 421–436 (2015). https://doi.org/10.1016/j.cmpb.2015.09.003
12. Vigueras-Guillén, J.P., Andrinopoulou, E.R., Engel, A., Lemij, H.G., van Rooij, J., Vermeer, K.A., van Vliet, L.J.: Corneal endothelial cell segmentation by classifier-based merging of oversegmented images (2018, submitted)